Tuning two-dimensional band structure of Cu(111) surface-state electrons that interplay with artificial supramolecular architectures

Shiyong Wang,[1] Weihua Wang,[1] Liang Z. Tan,[2] Xing Guang Li,[3] Zilang Shi,[1] Guowen Kuang,[1] Pei Nian Liu,[3] Steven G. Louie,[2,4] and Nian Lin[1,*]

[1]*Department of Physics, The Hong Kong University of Science and Technology, Hong Kong, China*
[2]*Department of Physics, University of California, Berkeley, CA 94720-7300, USA and Material Sciences Division, Lawrence Berkeley National Laboratory, Berkeley, CA 94720, USA*
[3]*Shanghai Key Laboratory of Functional Materials Chemistry and Institute of Fine Chemicals, East China University of Science and Technology, Meilong Road 130, Shanghai, China*
[4]*Institute for Advanced Study, Hong Kong University of Science and Technology, Hong Kong, China*

(Received 14 July 2013; revised manuscript received 24 November 2013; published 19 December 2013)

We report on the modulation of two-dimensional (2D) bands of Cu(111) surface-state electrons by three isostructural supramolecular honeycomb architectures with different periodicity or constituent molecules. Using Fourier-transformed scanning tunneling spectroscopy and model calculations, we resolved the 2D band structures and found that the intrinsic surface-state band is split into discrete bands. The band characteristics including band gap, band bottom, and bandwidth are controlled by the network unit cell size and the nature of the molecule-surface interaction. In particular, Dirac cones emerge where the second and third bands meet at the K points of the Brillouin zone of the supramolecular lattice.

DOI: 10.1103/PhysRevB.88.245430 PACS number(s): 73.20.At, 31.15.ae, 68.37.Ef, 73.63.Kv

I. INTRODUCTION

Two-dimensional electron gas (2DEG) confined in nanostructures on the close-packed faces of noble metals has enabled researchers to realize artificial quantum dots and demonstrate control of electronic structure at the nanoscale.[1–11] The nanostructures that scatter surface-state electrons can be built by scanning tunneling microscope (STM) manipulation of adatoms or molecules[1–5] or by self-assembly processes.[6–11] In recent years, the concepts of supramolecular coordination chemistry have been used to build two-dimensional systems through surface-assisted coordination assembly.[12,13] Highly ordered nanostructures consisting of metal atoms and organic molecules can form on surfaces according to well-defined metal-ligand coordination. In particular, one can apply the rational design principle to tune the lattice dimension and symmetry of the 2D systems.[14] This method has become an effective strategy for creating scaterring potentials for 2DEG. Two groups reported on the formation of 2D surface-state bands associated with periodical nanoporous supramolecular networks.[10,11] A particular interesting example of modulated 2DEG is a graphene-like Dirac fermion, as predicted in Refs. 15 and 16. Recently, Gomes *et al*. fabricated artificial graphene through STM manipulation of CO molecules on a Cu(111) surface and detected signatures of Dirac fermions using tunneling spectroscopy.[17] These studies demonstrate that artificial electronic band structures can be designed through nanostructuring noble metal surfaces with molecular architectures. As an analogue to photonic structures for electromagnetic waves, the realization of tunable electronic structures, which exhibit exotic charactreristics such as Dirac fermions, topological insulators, or anomalous quantum Hall states,[18–20] is of high interest in fundamental research, as well as in practical applications.

Here we report a systematic study of three isostructural honeycomb supramolecular network architectures used to modulate the 2DEG on a Cu(111) surface. We used Fourier-transformed scanning tunneling spectroscopy and model calculations to resolve the band structures of the 2DEG.[21–25] We determined quantitatively how the band bottom, bandwidth, and band gap are tailored by the periodicity of the supramolecular networks and by the molecule-substrate interaction. Moreover, we found that two bands touch at the K points of the network Brillouin zone, forming Dirac cones. Our results examplify how to create new quantum states out of 2DEG by changing both the geometry and the intermolecular bonding nature of artificial molecular systems.

II. EXPERIMENTAL AND THEORETICAL METHODS

Sample preparation and STM characterization were performed in a commercial ultrahigh vacuum ($\sim 10^{-10}$ mbar) tunneling microscope system (Omicron). A single-crystal Cu(111) was cleaned by cycles of Ar^+ ion sputtering and annealing to 800 K. We employed the metallo-supramolecular self-assembly method to construct the 2D architectures. 1,3,5-tris(pyridyl)benzene (M1), 1,3,5-tris[4-(pyridin-4-yl)phenyl]benzene (M2) and 1,3,5-tris(4-bromophenyl)benzene (M3) [cf. insets of Fig. 1(a)–1(c)] were deposited on the Cu(111) surface, which was held at room temperature using an organic molecular beam deposition source at 210, 370, and 250 °C respectively. After annealing at 120 °C, the samples were characterized at cryogenic temperature (4.9 K). The STM topographic data were acquired in constant current mode. The differential tunneling spectra dI/dV were measured using a lock-in amplifier with a sine modulation of 1.5 kHz at 5 mV.

To simulate the 2DEG band structures, we first calculated the effective potentials of the supramolecular systems using density functional theory (DFT) calculations as depicted in Fig. 1(d). These calculations were performed in a plane-wave basis set, using a 60 Ry kinetic energy cutoff, norm-conserving pseudopotentials, and a Perdew-Burke-Ernzerhof (PBE) exchange-correlation

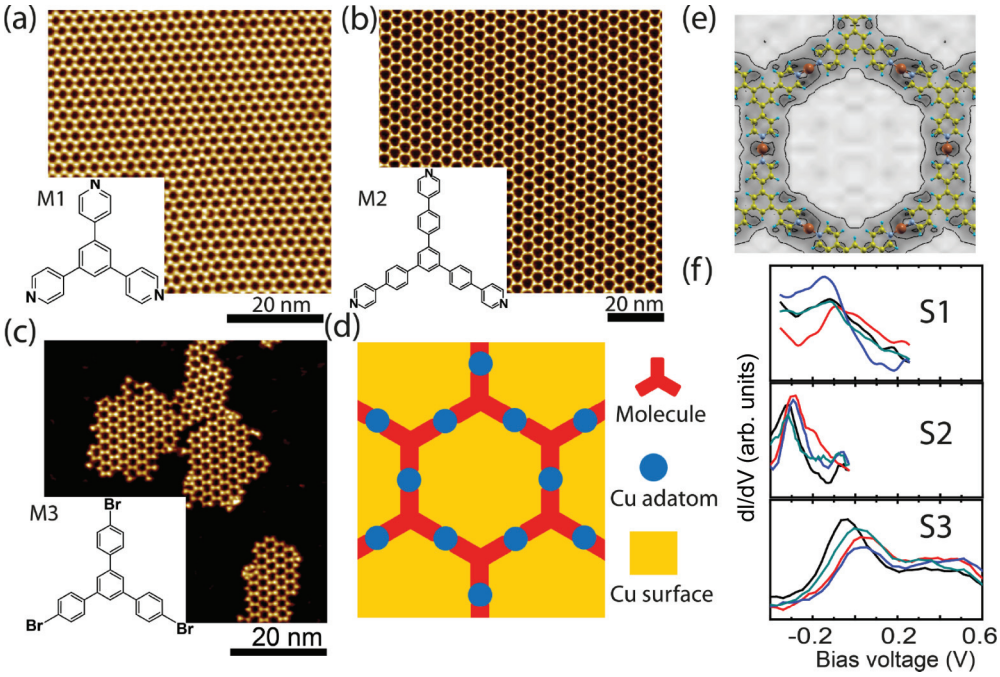

FIG. 1. (Color online) (a)–(c) STM topographic images (0.5 nA; 1.0 V) showing three isostructural supramolecular honeycomb networks. Insets: chemical structure of the molecule used to assemble the structures. (d) Structural model of the networks. (e) Effective potential seen by a surface state electron as calculated by DFT. (f) dI/dV spectra recorded at the center of four different pores in S1 (top), S2 (middle), and S3 (bottom) structures.

energy functional. Then we used two methods to calculate the 2D band structures. In method I, we solved Schrödinger's equation of a single electron inside a 2D periodic potential using plane waves and Bloch's theorem. In method II, we carried out jellium model calculations. The effective electron mass used is $0.4m_e$. Consistent results were obtained by the two methods.

III. RESULTS AND DISCUSSION

As shown in Fig. 1(a) and 1(b), the self-assembly of M1 or M2 resulted in large domains of network architectures with a honeycomb motif stabilized via pyridyl-Cu-pyridyl coordination bonds,[26,27] and denoted S1 or S2, respectively. M3 molecules underwent debromination and formed a honeycomb organometallic structure [cf. Fig. 1(c)] in which the neighboring molecules are linked by C-Cu-C bonds,[28] denoted S3. The domain size of this structure is smaller than that of M1 or M2, presumably due to the fact that the stronger organometallic bonds restrict the development of large networks in the self-assembly process. Figure 1(d) illustrates the common structural characters of the three honeycomb networks, where red three-arm stars represent the molecules and blue dots the Cu adatoms. The effective potential provided by the molecules and Cu atoms seen by a surface state electron, as shown in Fig. 1(e), was estimated from DFT calculations.

Figure 1(f) shows the differential tunneling (dI/dV) spectra, which represent the local density of states (LDOS) of the 2DEG, with the tip located at the center of four randomly selected pores for each of the three structures. These spectra display a broad peak, indicating that the Cu(111) surface electrons are modulated by the supramolecular structures. The rather broad peak suggests in part imperfect confinement provided by the pore boundary.[2,7–9,29,30] The peaks of the S2 spectra are at lower energy compared with those of S1, which can be associated with the larger area of the pore.[9] Although S3 is of a same periodicity as S1, its spectra have a peak at relative higher energy, implying that M3 provides a different scattering potential. Interestingly, in all three cases, different pores exhibit peaks of different characteristics (e.g., relative peak intensities, peak shape, and peak positions). We ruled out the possibility that these variations were associated with tip conditions or off-center tip location while acquiring the spectra.

To systematically probe the variation of the LDOS in different pores, we acquired dI/dV spectra, point by point (150×150 each frame), over large areas of the network structures. The real-space LDOS maps at given energies were then constructed by extracting the intensity of 150×150 individual point spectra at those energies. Figure 2(a) shows the LDOS maps at two selected energies of S1. One can see that the -296-mV LDOS map shows that the LDOS intensity is not uniformly distributed for different pores, confirming the dI/dV variation observed in Fig. 1(f). At a higher energy of -233 mV, more pores exhibit higher intensity. Figure 2(b) shows two LDOS maps at the selected energies of S2 structure exhibit similar behavior as those of S1. Figure 2(d) displays the Fourier-transformed LDOS (FT-LDOS) maps of S1 at nine incremental energies, which reveal energy-dependent evolution of LDOS intensity distribution in reciprocal (momentum) space: At low energies, the high-intensity spots are concentrated in the low-wave-vector region; with increasing energy, the intensity gradually expands to larger wave vector

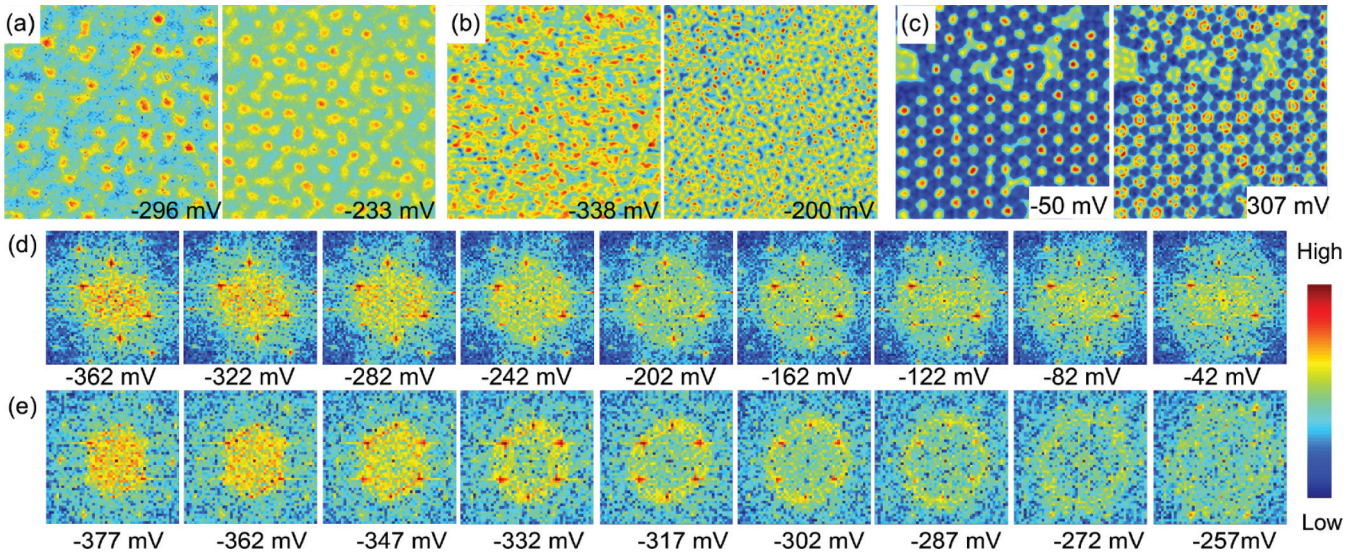

FIG. 2. (Color online) (a)–(c) LDOS maps of S1 (25 nm × 25 nm), S2 (60 nm × 60 nm), and S3 (25 nm × 25 nm) acquired at the defined energies. (d), (e) FT-LDOS maps of S1 ($10\ \mathrm{nm}^{-1} \times 10\ \mathrm{nm}^{-1}$) and S2 ($7\ \mathrm{nm}^{-1} \times 7\ \mathrm{nm}^{-1}$) at nine incremental energies.

regions. Note that the hexagonal spots are the reciprocal lattice vectors of the honeycomb lattice. Figure 2(e) displays nine FT-LDOS maps of S2 structure. One can see clearly that a ring-like feature appears at −347 mV and expands with increasing energy. Figure 2(c) shows the LDOS maps of the S3 structure at two energies. One can see in these pores that a dot appears at −50 mV and a ring appears at 307 mV. Since the domain size of the S3 networks is not large enough, it is difficult to do the same Fourier transformation analysis for S3. A detailed inspection, however, reveals that the LDOS intensity distribution is not homogeneous for different pores.

FT-LDOS maps have been widely used to image the band dispersions of a variety of systems.[21–25] Here we provide calculations showing that the FT-LDOS can be used to image the band dispersions in our supramolecular networks. The FT-LDOS is sensitive to scattering transitions of electrons within a constant energy contour (assuming elastic scattering). In this experiment, defects or impurities on the Cu(111) surface are the likely cause of the elastic scattering, because the Cu(111) surface band can be imaged under FT-LDOS, in the absence of the supramolecular networks. We assume that the scattering matrix elements are slowly varying in k space, since they are likely to be caused by short-range scattering. The FT-LDOS can then be approximated by a joint density of states calculation (Ref. 24). In Fig. 3, we show the results of such a calculation for a 2D electron gas, and for the S1 and S2 supramolecular structures using the DFT-estimated model potential.

We have constructed the energy dispersion in momentum space from the experimental FT-LDOS maps. For each energy within the measured energy range, we averaged the FT-LDOS signal over all wave vectors of equal magnitude (radial averaging of FT-DOS maps) to compile power spectra as a function of wave vector and energy. The results for S1 and S2 are shown in Figs. 4(a) and 4(b), respectively. Both spectral functions display a dispersive band in the Brillouin zone of the honeycomb networks (NBZ; the white dashed lines define the K and M points of the NBZ). As a reference, the power spectral function of the clean Cu(111) surface, which was obtained following the same procedure, is shown in Fig. 4(c). The dispersion of the 2DEG of the clean Cu (111) is plotted as the red dotted parabolas in Figs. 4(a) and 4(b). One can see that the band bottom of S1 is at −0.34 V, upwardly shifted by 60 meV compared with the clean Cu(111) 2DEG. The band bottom of S2 is at −0.37 V. The intensity of both bands is significantly reduced at the NBZ boundary. Similar measurements on clean Cu(111) do not show such intensity reductions, which excludes the possibility that the intensity

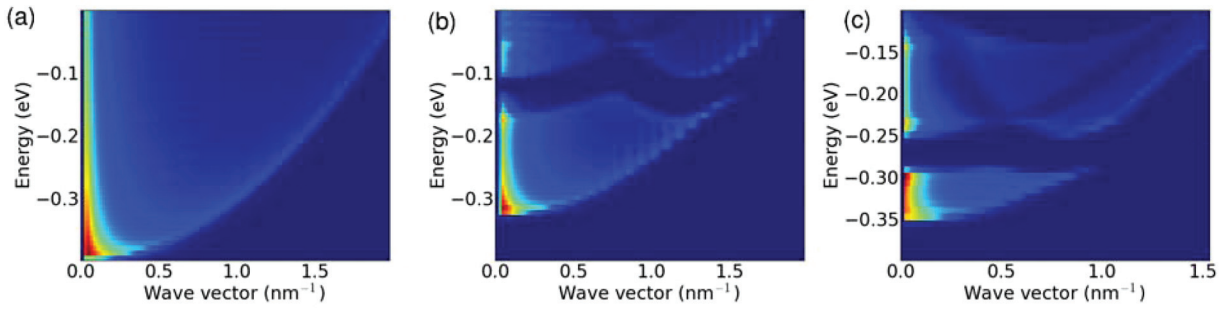

FIG. 3. (Color online) FT-LDOS calculations for (a) a 2D electron gas, (b) the S1 network, and (c) the S2 network. All plots are along the ΓK direction.

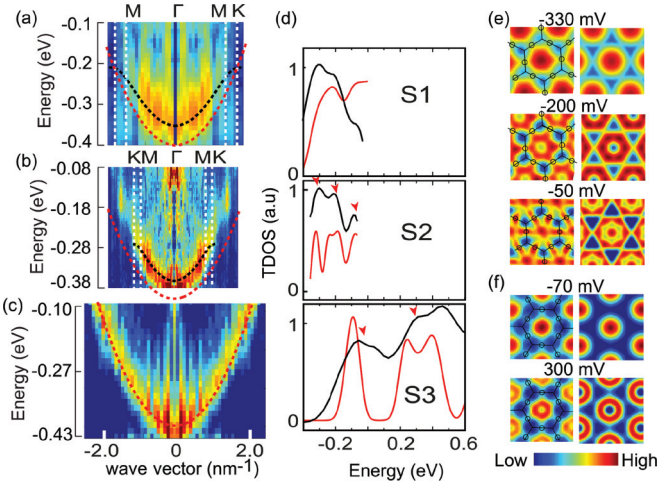

FIG. 4. (Color online) (a)–(c) Power spectral functions of 2DEG of S1, S2 (the supramolecular lattice spots are subtracted for clarity), and clean Cu(111) from top to bottom. Black dotted lines, simulated first band; red dotted lines, dispersion of Cu(111) surface state. (d) Experimental (black curve) and simulated (DFT-estimated potential) TDOS of S1 (top), S2(middle), and S3(bottom). (e), (f) Experimental (left) and simulated (right) unit-cell-averaged LDOS maps of S2 (8 nm × 8 nm) and S3 (5 nm × 5 nm) at the given energies. The inserted model is a guide for the eye.

reduction is due to low tunneling matrix elements. We attribute this feature to a finite bandwidth: S1 has a band from −0.34 to −0.22 V, and S2 has a band from −0.37 to −0.28 eV. These experimental findings provide clear evidence that the periodical supramolecular architectures modulate the Cu(111) surface-state electrons to form different dispersive 2D bands.

In our model calculations, we have used two different effective scattering potentials to model the molecules and Cu adatoms. The shape of the first potential, which has been estimated by the DFT total potential, is depicted in Fig. 1(d). We have evaluated the DFT total potential [Fig. 1(e)] on a plane at a distance of 3 Å from the molecules. For S1 and S2, the model molecular potential (red region with width 4.9 Å) is set as $V_m = 0.3$ eV, and the Cu potential (blue region with diameter 3.5 Å) $V_{Cu} = -0.1$ eV, since Cu is slightly positively charged in the coordination bond. For S3, we set $V_m = V_{Cu} = 0.9$ eV, accounting for the covalent nature of the organometallic bond, which is expected to change the nature of the molecule-surface interaction and thus the effective potential. We compare the results of using this effective potential with a second effective potential, where the molecules and Cu adatoms are represented by muffin-tin potentials of diameter 4.9 and 3.5 Å, with the same values of potential depth as above, respectively. The simulated first band along ΓK direction of S1 and S2 are shown as black dotted curves in Figs. 4(a) and 4(b). Both methods reproduce the experimentally resolved band dispersions fairly well for both S1 and S2 within the first NBZ. We also evaluated the total density of states (TDOS) of the three structures. Experimental TDOS were obtained through integrating the dI/dV spectra of the entire area. As shown in black curves in Fig. 4(d), the TDOS of S1 displays a broad peak at −0.3 eV and two shoulders at −0.2 and −0.05 eV; the TDOS of S2 has three peaks at −0.3, −0.2, and −0.1 eV and two dips at −0.25 and −0.15 eV; The TDOS of S3 has two peaks (−0.1 and 0.52 eV), two shoulders (0.05 and 0.45 eV), and a dip (0.15 eV). The red curves in Fig. 3(d) are simulated TDOS using the DFT-estimated potential (with a 25 mV broadening) of the three structures, showing fair agreement with the experimental TDOS. Upon comparison to the band structure, the TDOS peaks are associated with the first, the second, and the higher order bands; the dips are associated with the band gaps.

To better understand the band characteristics, we examine the LDOS maps averaged over the unit cells in a given sample. Figure 4(e) left panels are the unit-cell-averaged LDOS maps of S2 at the energies that are marked by the red arrow in Fig. 4(d). The −330 meV map shows a domelike feature at the pore center, which corresponds to the states of the first band. Upon increasing energy to −200 meV, a hexagon with a dip at the center appears, which can be assigned to the states of the second band. At −50 meV, a protrusion in the center and six bright spots in the hexagonal corner appear, which can be assigned to the states of the higher bands. Figure 4(f) left panels show the unit-cell-averaged LDOS maps of the S3 structure at two energies corresponding to the red arrows in Fig. 4(d). The domelike and the hexagon feature at −70 and 300 meV can be assigned to the states of the first and the second bands, respectively. The simulated LDOS intensity maps, calculated from the DFT-estimated potential, are shown in the right panels in Figs. 4(e) and 4(f), which reproduce the general features of the experimental results. We have found that the LDOS calculated from both model potentials give good agreement with experimental results at low energies, while the DFT-estimated potential is more accurate than the muffin-tin potential at higher energies because of the importance of higher Fourier components in that energy range.

The full band structures of the three structures calculated with the DFT-estimated potentials are plotted in Figs. 5(a)–5(c). The interplay of the artificial supramolecular architectures with the surface-state electrons tunes the band structure in three aspects: shifting the band bottom and varying the bandwidth and the band gap size. We now discuss the general trends exhibited by the band characteristics depending on the unit cell length of the supramolecular lattice and the effective potential. In the 2DEG model, the extent to which the periodic potential affects the surface state can be quantified by a dimensionless parameter $\zeta = \frac{m}{(2\pi\hbar)^2} V_1 L^2$, where L characterizes the unit cell length and V_1 the first Fourier component of the potential.[16] For the band bottom, it is offset from the Cu(111) surface state band bottom by the average value of the potential in the unit cell. We thus expect that S3, which has a larger band bottom offset than S1, provides a higher potential. We also expect that S1, which has a greater proportion of the unit cell occupied by the molecules, has a larger band bottom offset than S2. Both of these expectations are verified by our experiments. The parameter ζ also explains why S3, which has an identical configuration as S1, has a larger band gap. For a given potential, it was reported that the band gap is enlarged as the network pore size is reduced.[8,9] However, we find that when the unit cell size is below a critical value, the trend can be reversed. A similar trend for band gap as a function of potential strength was reported in Ref. 31. In Fig. 5(d), the calculated band gaps of 14 supramolecular network structures

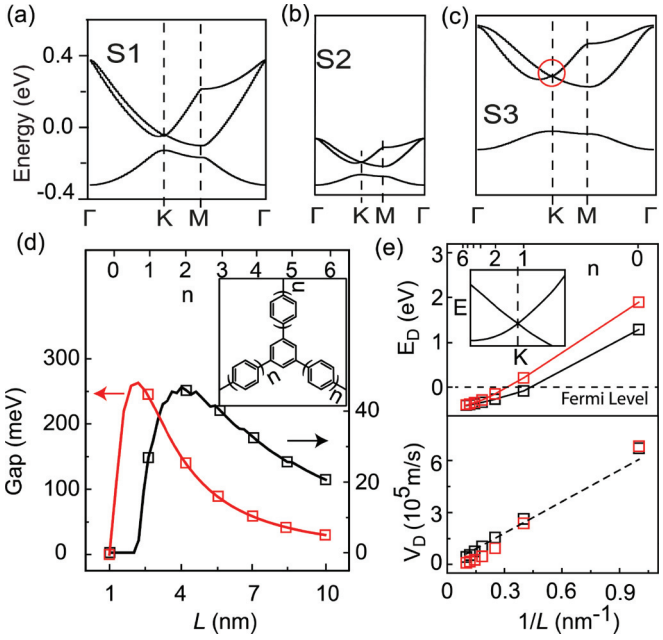

FIG. 5. (Color online) (a)–(c) Calculated (DFT-estimated potential) band gaps as a function of the unit cell size (L) of 14 supramolecular networks. Different values of L correspond to different numbers (n) of benzene rings in the arms of the network. (d) Calculated band gaps and (e) Dirac point energy and carrier velocity of 14 supramolecular networks. The black (red) squares denote the weak (strong) potential. The inset in the upper panel shows the magnified view of the red circle in S3. The dashed line in the low panel indicates the result obtained from $k \cdot p$ theory.

with increasing size are plotted (the molecular model is shown in the inset). The critical unit cell length is ~4 nm for the weak potential ($V_m = 0.3$ eV) and ~2.5 nm for the strong potential ($V_m = 0.9$ eV). The effective potential in the limit of $L \to 0$ is almost homogeneous because the molecular backbone [see inset of Fig. 4(d)] occupies an increasingly large proportion of the unit cell, and the pores become vanishingly small as L approaches zero. Consequently, the band dispersion should be free electron-like and gapless in this limit. For the smallest molecule in our calculations, the pores occupy only 19% of the unit cell area; the first and second bands overlap, and the band gap disappears.

The circled region in Fig. 5(c), where the second and the third bands meet at K points, is magnified in the inset in Fig. 5(e). For a small nonzero momentum deviation, q, away from the K points, a linear dispersion emerges, and the two bands form Dirac cones at the K points.[16,32] We can define $E(K+q) = E_D + \frac{\hbar^2 q^2}{2m^*} + \hbar q v_D$, where E_D is the energy level of the Dirac point and v_D the carrier velocity. Note this type of massless quasi-particle is different from those in graphene, considering other states are present at the same energy in other parts of the Brillouin zone. The upper panel of Fig. 5(e) displays the calculated E_D of the 14 supramolecular networks. One can see that increasing the unit cell size L can downshift E_D below the Fermi energy of Cu(111). In other words, the Dirac cones can be doped effectively by tuning the network periodic length: The Dirac cone is p-doped for $n = 0$ and 1 (strong potential) or $n = 0$ (weak potential), and n-doped in all other situations, where n is defined as the number of benzene rings in the arms of the molecules [see Fig. 5(d)]. The lower panel of Fig. 5(e) shows the calculated v_D as a function of inverse L, which agrees with the result of $k \cdot p$ perturbation theory, $v_D = \frac{h}{3m^* L}$.[12,16,30]

IV. CONCLUSIONS

We find that three isostructural supramolecular architectures on Cu(111) with variable periodical length and molecule-surface interaction can result in 2D bands of tunable band characteristics. These results demonstrate that self-assembled supramolecular structures, which can be created easily and rapidly in the laboratory, provide an effective means to control and manipulate artificial 2D electronic structures.

ACKNOWLEDGMENTS

This work is supported in part by the Hong Kong RGC (D-HK008/11T) and the U.S. National Science Foundation Grant No. DMR10-1006184. S.G.L. acknowledges support of a Simons Foundation Fellowship in Theoretical Physics. We acknowledge the assistance of the XSEDE computational cluster resource provided by NICS (kraken), supported by the National Science Foundation

* Corresponding author: phnlin@ust.hk

[1] M. F. Crommie, C. P. Lutz, and D. M. Eigler, Science **262**, 218 (1993).
[2] H. C. Manoharan, C. P. Lutz, and D. M. Eigler, Nature **403**, 512 (2000).
[3] J. Kliewer, R. Berndt, and S. Crampin, Phys. Rev. Lett. **85**, 4936 (2000).
[4] C. R. Moon, L. S. Mattos, B. K. Foster, G. Zeltzer, and H. C. Manoharan, Nature Nanotechnol. **4**, 167 (2009).
[5] C. Didiot, S. Pons, B. Kierren, Y. Fagot-Revurat, and D. Malterre, Nature Nanotechnol. **2**, 617 (2007).
[6] J. Li, W.-D. Schneider, R. Berndt, and S. Crampin, Phys. Rev. Lett. **80**, 3332 (1998).
[7] Y. Pennec, W. Auwärter, A. Schiffrin, A. Weber-Bargioni, A. Riemann, and J. V. Barth, Nature Nanotechnol. **2**, 99 (2007).
[8] F. Klappenberger, D. Kühne, W. Krenner, I. Silanes, A. Arnau, F. J. García de Abajo, S. Klyatskaya, M. Ruben, and J. V. Barth, Nano Lett. **9**, 3509 (2009).
[9] F. Klappenberger, D. Kühne, W. Krenner, I. Silanes, A. Arnau, F. J. García de Abajo, S. Klyatskaya, M. Ruben, and J. V. Barth, Phys. Rev. Lett. **106**, 026802 (2011).
[10] J. Lobo-Checa, M. Matena, K. Müller, J. H. Dil, F. Meier, L. H. Gade, T. A. Jung, and M. Stöhr, Science **325**, 300 (2009).
[11] R. Stiufiuc, L. M. A. Perdigão, B. Grandidier, D. Deresmes, G. Allan, C. Delerue, D. Stiévenard, P. H. Beton, S. C. Erwin,

M. Sassi, V. Oison, and J.-M. Debierre, Phys. Rev. B **81**, 045421 (2010).
[12]S. Stepanow, N. Lin, and J. V. Barth, J. Phys.: Condens. Matter **20**, 184002 (2008).
[13]N. Lin, S. Stepanow, M. Ruben, and J. V. Barth, Top. Curr. Chem. **287**, 1 (2009).
[14]S. Stepanow, M. Lingenfelder, A. Dmitriev, H. Spillmann, E. Delvigne, N. Lin, X. Deng, C. Cai, J. V. Barth, and K. Kern, Nat. Mater. **3**, 229 (2004).
[15]C.-H. Park and S. G. Louise, Nano Lett. **9**, 1793 (2009).
[16]M. Gibertini, A. Singha, V. Pellegrini, M. Polini, G. Vignale, A. Pinczuk, L. N. Pfeiffer, and K. W. West, Phys. Rev. B **79**, 241406(R) (2009).
[17]K. K. Gomes, W. Mar, W. Ko, F. Guinea, and H. C. Manoharan, Nature **483**, 306 (2012).
[18]P. Ghaemi, S. Gopalakrishnan, and T. L. Hughes, Phys. Rev. B **86**, 201406(R) (2012).
[19]F. de Juan, Phys. Rev. B **87**, 125419 (2013).
[20]O. P. Sushkov and A. H. Castro Neto, Phys. Rev. Lett. **110**, 186601 (2013).
[21]L. Petersen, Ph. Hofmann, E. W. Plummer, and F. Besenbacher, J. Electron Spectrosc. Relat. Phenom. **109**, 97 (2000).
[22]G. M. Rutter, J. N. Crain, N. P. Guisinger, T. Li, P. N. First, and J. A. Stroscio, Science **317**, 219 (2007).
[23]F. Vonau, D. Aubel, G. Gewinner, S. Zabrocki, J. C. Peruchetti, D. Bolmont, and L. Simon, Phys. Rev. Lett. **95**, 176803 (2005).
[24]L. Simon, C. Bena, F. Vonau, M. Cranney, and D. Aubel, J. Phys. D: Appl. Phys. **44**, 464010 (2011).
[25]J. E. Hoffman, K. McElroy, D.-H. Lee, K. M. Lang, H. Eisaki, S. Uchida, and J. C. Davis, Science **297**, 1148 (2002).
[26]J. Liu, T. Lin, Z. Shi, F. Xia, L. Dong, P. N. Liu, and N. Lin, J. Am. Chem. Soc. **133**, 18760 (2011).
[27]Z. Shi, J. Liu, T. Lin, F. Xia, P. N. Liu, and N. Lin, J. Am. Chem. Soc. **133**, 6150 (2011).
[28]W. Wang, X. Shi, S. Wang, M. Van Hove, and N. Lin, J. Am. Chem. Soc. **133**, 13264 (2011).
[29]J. Kliewer, R. Berndt, and S. Crampin, New J. Phys. **3**, 22 (2001).
[30]H. Jensen, J. Kröger, R. Berndt, and S. Crampin, Phys. Rev. B **71**, 155417 (2005).
[31]E. Räsänen, C. A. Rozzi, S. Pittalis, and G. Vignale, Phys. Rev. Lett. **108**, 246803 (2012).
[32]N. Y. Kim, K. Kusudo, A. Loeffler, S. Hoefling, A. Forchel, and Y. Yamamoto, New J. Phys. **15**, 035032 (2013).